Stereo PIV Measurements of Low-Aspect-Ratio Low-Reynolds-Number Wings with Sinusoidal Leading Edges for Improved Computational Modeling

H. E. C. Delgado[1], A. Esmaeili[2] and J. M. M. Sousa[3]
Instituto Superior Técnico, 1049-001 Lisbon, Portugal

Stereo Particle Image Velocimetry measurements of the flow field around a unity aspect ratio wing with a sinusoidal leading-edge have been carried out at a Reynolds number Re = 140, 000 for two angles of attack, α = 0º and 15º. These measurements are intended to be used for improved computational modeling of the flow employing Detached Eddy Simulations. For this reason, numerical predictions have also been carried out for the mentioned flow cases, using the "F2-shielded" modeling and the "delayed" modeling approaches for the SST k-ω turbulence model, as well as a reference Reynolds-Averaged Navier-Stokes calculation. The results have demonstrated the superior performance of the "delayed" modeling at high incidence. However, the latter approach unexpectedly fails at low incidence, hence indicating the need for improved boundary layer transition modeling.

Nomenclature

AR	=	aspect ratio
α	=	angle of attack
C_L	=	lift coefficient
c	=	wing chord, m
Re	=	Reynolds number

I. Introduction

MICRO air vehicles generally make use of low aspect ratio wings and, as a consequence of their small size and low flight velocities, they operate in the low Reynolds number regime (Re < 200,000).[1] This is especially challenging for aerodynamicists as laminar separation and early stall plague this regime of operation, eventually compromising the performance of the vehicle and demanding elaborate computational modeling at design stages. On the other hand, it has been demonstrated a few years ago that stall control in airfoils may be attained via a sinusoidal modification of their leading edges, with little or no drag penalty.[2,3] The original idea was inspired in biomimetics, namely following the observation that the pectoral flippers of the "acrobatic" humpback whales[4] exhibited scalloped leading edges.[5] For this reason, other studies focused on very specific high-aspect ratio tapered wings as an attempt to mimic a real whale flipper, both from the experimental[6] and computational points of view.[7] Numerical predictions of the flow around baseline and modified airfoils in Ref. 3 have lately been performed employing a Reynolds-Averaged Navier-Stokes (RANS) approach.[8] Very recently, Particle Image Velocimetry measurements have been carried out as well for a different airfoil geometry,[9] bringing additional insight about the physical mechanisms behind this type of flow control.

The promising results initially reported for airfoils were also the subject of detailed wind tunnel studies aimed at extending the analysis to low-aspect-ratio low-Reynolds-number wings,[10] and thus envisaging the application of the technique to fixed-wing micro aerial vehicles. Among other results, these studies identified the appearance of locally separated flow, even at relatively low incidences, not only as a consequence of the use of rather thick wing sections but namely resulting from the leading-edge modification. Such experimental observations were later partially confirmed via numerical simulation of the foregoing experiments employing Detached Eddy Simulations (DES).[11]

---

[1] Graduate Student, Department of Mechanical Engineering, Avenida Rovisco Pais.
[2] Graduate Student, Department of Mechanical Engineering, Avenida Rovisco Pais.
[3] Associate Professor, Department of Mechanical Engineering, Avenida Rovisco Pais, Associate Fellow AIAA.

Figure 1 shows that one of the outcomes of using a sinusoidal leading-edge is the local intensification of the suction peak at the *valleys*, hence potentially leading to the establishment of a three-dimensional separation bubble.

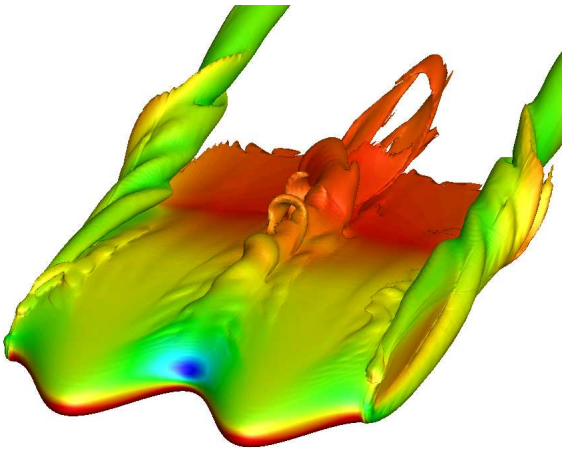

Figure 1: Instantaneous flow field for a unity aspect ratio wing with a sinusoidal leading-edge at Re = 160,000 and α = 15°. Color contours and iso-surfaces represent pressure coefficient and vorticity, respectively.[11]

The above results demonstrate that additional difficulties may be expected in the simulation of the low-Reynolds-number flow around this type of finite wings. Advanced simulation techniques such as DES are likely to be the most adequate choice to cope with the complexities of both the flow and wing geometry. However, although the gross features of the flow physics may already have been reproduced in the aforementioned simulations,[11] it was concluded that improved computational modeling is still required for an accurate prediction of the aerodynamic characteristics.

The main objective of the present work is to employ Stereo Particle Image Velocimetry (SPIV) measurements to assist the improvement of DES modeling. Hence, detailed three-component velocity data are obtained at various incidences and the velocity maps are compared with the corresponding results produced by different numerical simulation approaches.

II. Wind Tunnel Experiments

The present experiments were carried out at the low-speed, open-circuit wind tunnel described in Ref. 10, making use of the same wing models reported therein as well, which were based on the NASA LS(1)-0417 profile. Briefly, the wind tunnel has a test section with a cross-sectional area of 1.35×0.80 m^2, operating at undisturbed air velocities up to approximately 10 m/s; the wing models have a (mean) chord c = 232 mm for aspect ratios AR = 1 and 1.5, and varying values of amplitude and wavelength of the sinusoidal leading edges. However, at the current stage of the SPIV experiments, only model S1-LL (AR = 1, sinus amplitude 0.12c, sinus wavelength 0.50c) has been considered.

The basic characteristics of the SPIV system (Dantec Dynamics, Denmark) are as follows:

a) a DualPower 200-15 YAG laser (Litron, UK) operated at a frequency of 10 Hz with pulse energy of 2×190 mJ @ 532 nm;
b) two digital cameras FlowSense EO 4M with a resolution of 2048×2048 pixels equipped with objectives Macro Zeiss 50 mm;
c) data processing performed by the DynamicStudio software.

In order to maximize the field of view when the wings were positioned at moderate to high incidences, the first camera was installed perpendicularly to the laser light sheet (which, in turn, was perpendicular to the wing platforms) and the second was tilted to an angle of 34 degrees. Proper camera mounts and a fully computer-controlled 4-axis translation system (ISEL, Germany) allowed keeping the system aligned and focused in Scheimpflug condition during spanwise flow field surveys. Seeding was provided upstream of the wind tunnel plenum by a 1500 W commercial smoke generator with DMX control.

SPIV numerical data have been obtained using 32×32 pixels interrogation windows with an image overlap of 50% and applying two levels of multi-pass processing to increase the dynamic range of the measurements. The laser pulse separation was set to 10 ms, after optimization of image correlation for both cameras views.

III. Numerical Simulations

The numerical wing models were originally constructed using the CAD software Solidworks, based on the prescribed wing section. In order to generate the sinusoidal leading edge, the reference wing section had to be modified without distorting the trailing region. It was decided that the original airfoil should correspond to zero amplitude points in the sinus wave. Hence, the profiles located at smaller chord zones than the reference (*valleys*) have larger leading edge radii and the profiles corresponding to maximum amplitude zones, displaying larger chords (*peaks*), are relatively thinner than the reference geometry and have a smaller leading edge radius. The mean chord of all the models used in the present study was kept constant. A choice for square wing tips has been made and, as a consequence, the wing ends abruptly, which complicates the task of mesh generation. However, this option has the advantage of avoiding the addition of extra variables to the design of the models.

The computational mesh for finite wing simulations was generated employing a C-H-topology built with about 10 million mesh nodes. Far-field boundaries were set at a distance of approximately 20*c*. No-slip conditions were applied along the wall surfaces of the wing. Aiming to properly resolve the wall boundary layers, mesh nodes were clustered near wing surfaces using a geometric expansion. Finally, as the flow remained incompressible in all studied cases, a simple open boundary condition was used at the outflow section.

As initially discussed in Section I, taking into account the geometry of the models and the selected Reynolds number, DES seemed to be the most adequate approach to deal with the intrinsic complexities of the flow. Namely, DES is known to have a good performance when massive separations occur,[12] which is expected to arise for the models operating at high angles of attack. However, reference simulations employing RANS have been carried out as well. In both approaches the selected turbulence model was the SST k-ω,[13] mostly because of its superior performance at reducing the mesh influence of the DES limiter in the RANS boundary layer.[12] Briefly, the three following approaches have been analyzed:

a) standard RANS;
b) "shielded" DES, using function F2 of the SST k-ω turbulence model to preserve the RANS mode and avoid grid induced separation (DES-F2);
c) "delayed" DES, following a procedure[14] to delay the Large Eddy Simulation function using the SST k-ω turbulence model (DDES).

The numerical solution procedure used a SIMPLE (Semi-Implicit Method for Pressure Linked Equations) pressure-velocity coupling and a second-order accurate spatial discretization for the pressure. The QUICK (Quadratic Upwind Interpolation for Convective Kinematics) scheme was used in the discretization of momentum and turbulence equations.[15] However, the time integration was performed employing a second-order accurate implicit scheme to alleviate numerical stability restrictions. The time step used was 0.0025 s in all simulations. The numerical model chord and the free stream velocity were fixed to 250 mm and 8.18 m/s, respectively. This corresponded to a Reynolds number Re = 140,000, within the typical range of operation of MAVs. In a number of cases the simulations had to be carried out for longer than 40 s in order to reach a statistically converged unsteady behavior unaffected by initial transients.

IV. Results and Discussion

Experiments and simulations have been performed at two angles of attack for the model and flow conditions described in the previous sections. The first at an angle of attack $\alpha = 15^{\circ}$, for which a complex, separated flow was expected, and the second at $\alpha = 0^{\circ}$, for which only attached flow was anticipated.

A. Angle of attack $\alpha = 15^{\circ}$

The time-averaged velocity fields obtained at a central, vertical plane crossing the wing model are shown in Fig. 2 for both SPIV experiments and the three different numerical approaches listed in Section III. In all maps the velocities have been normalized by the free-stream velocities to facilitate a direct comparison.

The results clearly demonstrate the superior performance of DDES over DES-F2 and RANS. In fact the flow fields obtained for the latter two approaches are quite similar. The most striking difference between these numerical predictions and the results obtained with SPIV and DDES is that only a small separation is shown downstream of the suction peak at the leading-edge valley, whereas massive separation occurs in the trailing-edge region. SPIV and DDES data are very close, with this numerical approach apparently slightly under-predicting the size of the (upstream) separation bubble.

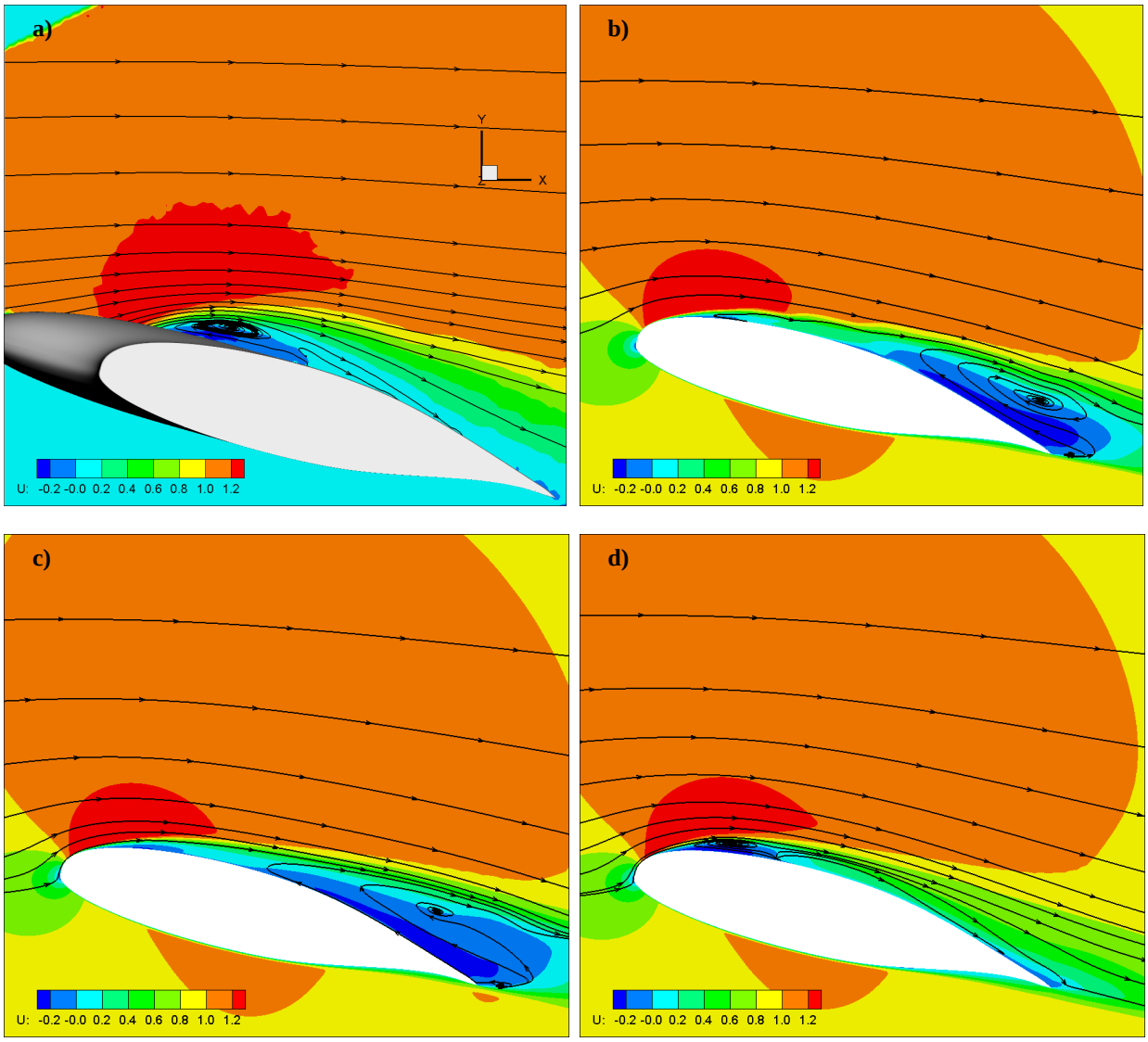

Figure 2: Time-averaged velocity fields obtained at the symmetry plane for *Re* = 140,000 and α = 15º; a) SPIV; b) RANS; c) DES-F2; d) DDES.

A three-dimensional (partial) view of this closed separation flow region shown in Fig. 3, aimed at more detailed comparisons with the numerical simulations, has been obtained with SPIV data. A total of 13 spanwise, vertical, time-averaged velocity maps, extending over a half of the wing model have been used in the three-dimensional reconstruction of the flow. The original experimental data has been interpolated into a regular mesh with the same spanwise spacing as that of SPIV interrogation windows. Again, when compared with the DDES predictions, the size of the (upstream) separation bubble is noted to be slightly larger, hence still demanding for improved numerical modeling. On the other hand, small separations can also be seen in the trailing-edge region, which was found to be in agreement with the DDES results as well (not shown here).

Rather unexpectedly, the deficiencies of RANS and DES-F2 models on reproducing the detailed flow physics at α = 15º do not significantly affect the calculation of the aerodynamic characteristic C_L, as shown in Fig. 4 in comparison with experimental data from Ref. 10. Much more surprising, however, are the difficulties exhibited by the DDES to cope with the seemingly easier case at α = 0º, as will be discussed in the next subsection.

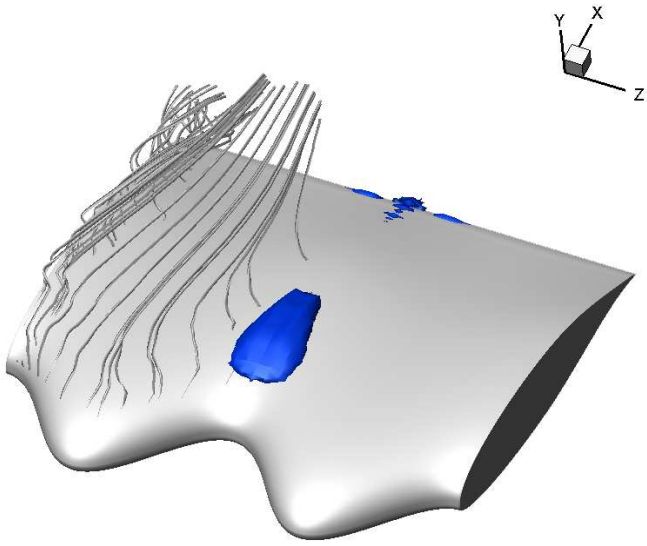

Figure 3: Three-dimensional reconstruction of the time-averaged flow field using SPIV data at *Re* = 140,000 and α = 15º. Iso-surfaces correspond to zero streamwise velocity.

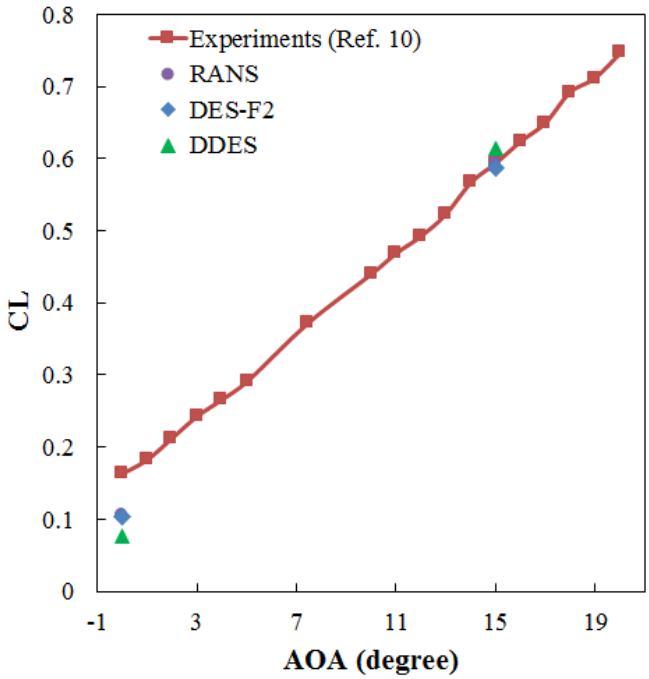

Figure 4: Lift coefficient data obtained at *Re* = 140,000 from aerodynamic balance measurements,[10] RANS, DES-F2 and DDES modeling.

B. Angle of attack α = 0º

The time-averaged velocity fields obtained at a central, vertical plane crossing the wing model are shown for the new incidence in Fig. 5, again for both SPIV experiments and the three different numerical approaches listed in Section III. Once more time, in all maps the velocities have been normalized by the free-stream velocities to facilitate a direct comparison.

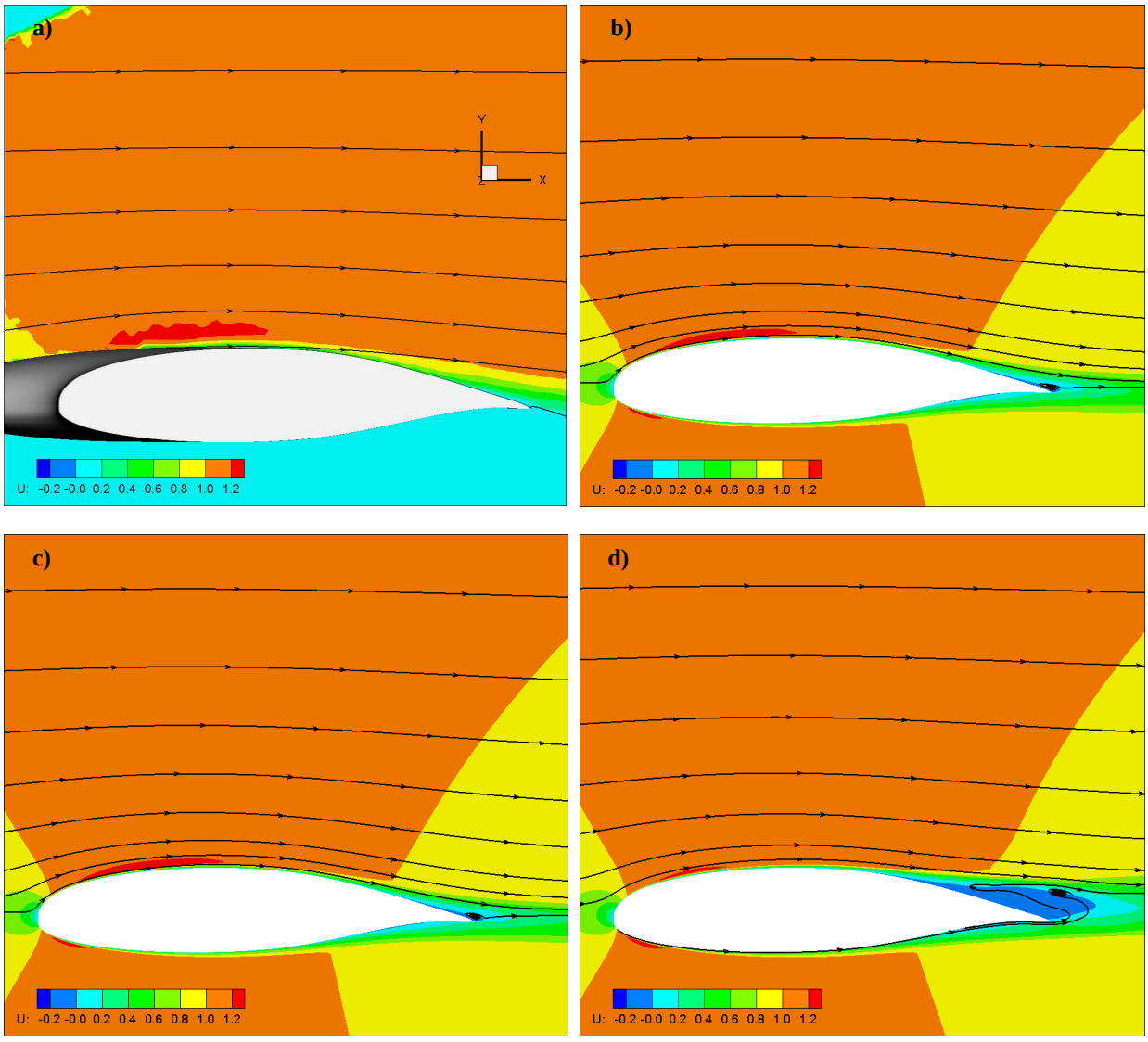

Figure 5: Time-averaged velocity fields obtained at the symmetry plane for *Re* = 140,000 and α = 0º; a) SPIV; b) RANS; c) DES-F2; d) DDES.

The results show that RANS and DES-F2 predictions are now much closer to SPIV velocity data, which does not show, as expected, any separation at this angle of attack. Apparently, in this case, the DDES model is not able to generate a turbulent boundary layer over the upper surface, leading to laminar separation at the trailing-edge. The turbulent separation obtained with the remainder models is much smaller, thus seemingly producing results that are closer to those obtained with SPIV. However, as seen before in Fig. 4, in order to better reproduce the aerodynamic balance measurements, further modeling improvements are still needed. Presumably, the laminar-turbulent transition prediction capabilities of the DDES must allow the development of a significant extent of the boundary layer in the laminar regime, but still avoiding laminar separation in the trailing-edge region. This is apparently confirmed by the SPIV data in Fig. 5, where the boundary layer, despite escaping separation, exhibits much larger deficits.

V. Conclusion

With the aim of providing a solid basis for the improvement of numerical modeling of the flow around low-aspect-ratio wings with sinusoidal leading-edges for stall control at low Reynolds number, Stereo PIV measurements have been carried out at *Re* = 140,000 for two angles of attack, α = 0º and 15º. Detached Eddy Simulations have also been performed for the mentioned flow cases, using the "F2-shielded" modeling and the

"delayed" modeling approaches for the SST k-ω turbulence model, as well as a reference Reynolds-Averaged Navier-Stokes calculation. Despite the minor differences in lift coefficient, best results were clearly obtained with the "delayed" modeling at high incidence, whereas the other models completely missed a correct reproduction of the flow physics. However, the former approach unexpectedly failed to meet our expectations at low incidence. In this case, better results were obtained with the remainder models. Nevertheless, all the results were globally worse than those obtained at high incidence, thus indicating the need for improved boundary layer modeling.

Acknowledgments

This work was funded by the Portuguese Government through "Fundação para a Ciência e a Tecnologia", in the scope of project NATURE (PTDC/EME-MFE/122849/2010).

References

[1]Mueller, T. J., and DeLaurier, J. D., "Aerodynamics of Small Vehicles," *Annu. Rev. Fluid Mech.*, Vol. 35, Jan., 2003, pp. 89-111.
doi: 10.1146/annurev.fluid.35.101101.161102

[2]Custodio, D. S., "The Effect of Humpback Whale-like Leading Edge Protuberances on Hydrofoil Performance," M.Sc. Thesis, Dept. of Mechanical Engineering, Worcester Polytechnic Institute, Worcester, MA, 2007.

[3]Johari, H., Henoch, C., Custodio, D., and Levshin, A., "Effects of Leading-Edge Protuberances on Airfoil Performance," *AIAA Journal*, Vol. 45, No. 11, 2007, pp. 2634-2641.
doi: 10.2514/1.28497

[4]Edel, R. K., and Winn, H. E., "Observations on Underwater Locomotion and Flipper Movement of the Humpback Whale *Megaptera novaeangliae*," *Marine Biology*, Vol. 48, No. 3, 1978, pp. 279-287.
doi: 10.1007/BF00397155

[5]Fish, F. E., and Battle, J. M., "Hydrodynamic Design of the Humpback Whale Flipper," *Journal of Morphology*, Vol. 225, No. 1, 1995, pp. 51-60.
doi: 10.1002/jmor.1052250105

[6]Miklosovic, D. S., Murray, M. M., Howle, L. E., and Fish, F. E., "Leading-edge Tubercles Delay Stall on Humpback Whale (*Megaptera novaeangliae*) Flippers," *Physics of Fluids*, Vol. 16, No. 5, 2004, pp. 39-42.
doi: 10.1063/1.1688341

[7]Pedro, H. T. C., and Kobayashi, M. H., "Numerical Study of Stall Delay on Humpback Whale Flippers," *46th AIAA Aerospace Sciences Meeting and Exhibit*, AIAA Paper 2008-0584, Jan. 2008.

[8]Dropkin, A., Custodio, D., Henoch, C. W., and Johari, H., "Computation of Flowfield Around an Airfoil with Leading-Edge Protuberances," *Journal of Aircraft*, Vol. 49, No. 5, 2012, pp. 1345-1355.
doi: 10.2514/1.C031675

[9]Zhang, M. M.., Wang, G. F., and Xu, J. Z., "Aerodynamic Control of Low-Reynolds-Number Airfoil with Leading-Edge Protuberances," *AIAA Journal*, Vol. 51, No. 8, 2013, pp. 1961-1971.
doi: 10.2514/1.J052319

[10]Guerreiro, J. L. E., and Sousa, J. M. M., "Low-Reynolds-Number Effects in Passive Stall Control Using Sinusoidal Leading Edges," *AIAA Journal*, Vol. 50, No. 2, 2012, pp. 461-469.
doi: 10.2514/1.J051235

[11]Câmara, J. F. D., and Sousa, J. M. M., "Numerical Study on the Use of a Sinusoidal Leading Edge for Passive Stall Control at Low Reynolds Number," *51st AIAA Aerospace Sciences Meeting*, AIAA Paper 2013-0062, Jan. 2013.
doi: 10.2514/6.2013-62

[12]Bunge, U., Mockett, C., and Thiele, F., "Guidelines For Implementing Detached-Eddy Simulation Using Different Models," *Aerospace Science and Technology*, Vol. 11, No. 5, 2007, pp. 376-385.
doi: 10.1016/j.ast.2007.02.001

[13]Menter, F. R., Kuntz, M., and Langtry, R., "Ten Years of Industrial Experience with the SST Turbulence Model," *Turbulence, Heat and Mass Transfer 4*, edited by Hanjalić, K., Nagano, Y., and Tummers, M., Begell House, Inc., New York, Wallingford (UK), 2003, pp. 625-632.

[14]Gritskevich, M.S., Garbaruk, A. V., Schütze, J. and Menter, F. R., "Development of DDES and IDDES for the k-ω Shear Stress Transport Model," *Flow, Turbulence and Combustion*, Vol. 88, 2012, pp. 431-449.
doi: 10.1006/jcph.1993.1087

[15]Pereira, J. C. F., and Sousa, J. M. M., "Finite Volume Calculations of Self-Sustained Oscillations in a Grooved Channel," *Journal of Computational Physics*, Vol. 106, No. 1, 1993, pp. 19-29.
doi: 10.1006/jcph.1993.1087